One-dimensional Rashba states with unconventional spin texture in Bi chains

P. M. Sheverdyaeva,[1] D. Pacilè,[2,*] D. Topwal,[3,4] U. Manju,[5] M. Papagno,[2] V. Feyer,[6] M. Jugovac,[1,6,†] G. Zamborlini,[6] I. Cojocariu,[6] C. Tusche,[6,7] X. L. Tan,[6] K. Hagiwara,[6] Y.-J. Chen,[6,7] J. Fujii,[8] P. Moras,[1] L. Ferrari,[9] E. Vescovo,[10] G. Bihlmayer,[11] and C. Carbone[1]

[1]*Istituto di Struttura della Materia-CNR (ISM-CNR), SS 14, Km 163,5, I-34149, Trieste, Italy*
[2]*Dipartimento di Fisica, Università della Calabria, 87036 Arcavacata di Rende (CS), Italy*
[3]*Homi Bhabha National Institute, Training School Complex, Anushakti Nagar, Mumbai 400094, India*
[4]*Institute of Physics, Sachivalaya Marg, Bhubaneswar 751005, India*
[5]*CSIR - Institute of Minerals and Materials Technology, Bhubaneswar 751013, India*
[6]*Peter Grünberg Institut PGI, Forschungszentrum Jülich, 52425 Jülich, Germany*
[7]*Fakultät für Physik, Universität Duisburg-Essen, Duisburg 47057, Germany*
[8]*Istituto Officina dei Materiali (IOM)-CNR, Laboratorio TASC, S.S.14, Km 163.5, 34149 Trieste, Italy*
[9]*Istituto di Struttura della Materia, Consiglio Nazionale delle Ricerche, 00133 Roma, Italy*
[10]*National Synchrotron Light Source, Brookhaven National Laboratory, Upton, New York 11973, USA*
[11]*Peter Grünberg Institut and Institute for Advanced Simulation, Forschungszentrum Jülich and JARA, D-52425 Jülich, Germany*

(Received 20 May 2022; accepted 16 June 2022; published 7 July 2022)

Spin-polarized electrons confined in low-dimensional structures are of high interest for spintronics applications. Here, we investigate the electronic structure of an ordered array of Bi monomer and dimer chains on the Ag(110) surface. By means of spin-resolved photoemission spectroscopy, we find Rashba-Bychkov split bands crossing the Fermi level with one-dimensional constant energy contours. These bands are up-spin polarized for positive wave vectors and down-spin polarized for negative wave vectors, at variance with the Rashba-Bychkov model that predicts a pair of states with opposite spin in each half of the surface Brillouin zone. Density functional theory shows that spin-selective hybridization with the Ag bulk bands originates this unconventional spin texture.

DOI: 10.1103/PhysRevB.106.045108

I. INTRODUCTION

The spin field-effect transistor proposed in the 1990s [1] opened a gateway to manipulate and use the spin of electrons for information technology [2,3]. Although efficient manipulation of electron spins in semiconductors has been achieved [4,5], reaching high spin-charge interconversion efficiency is still a challenge in spintronics research. An efficient conversion was reported in systems with strong spin-orbit interaction, either due to the Rashba-Bychkov (RB) effect in a two-dimensional (2D) electron gas [6,7] or due to the spin-momentum locking in the surface states of topological insulators (TIs) [8–12]. More recently, bulk systems with large spin-orbit splitting and one-dimensional (1D) electronic features were predicted to host exotic quantum phenomena [13–19]. In these systems, quasi-1D states exhibit a characteristic spin texture in k space that is locked along the 1D Fermi surface between opposite directions, thus preventing electron backscattering and generating robust spin currents. The creation of 1D systems with large spin-orbit splitting has been partially explored in the growth of heavy elements on (110) surfaces, e.g., Bi/InAs(110) [20], Bi(Pb)/Cu(110)[21], Bi/Au(110)[22], Bi/GaSb(110)[23] and Pt/Si(110)[24]. These quasi-1D Rashba systems were experimentally reported to exhibit interesting electronic effects caused by the reduced dimensionality, in particular nearly 1D contours, and giant conventional Rashba splitting. In conventional RB systems two channels of opposite spins are present at negative as well as at positive wave vectors [25,26]. This leads to a partial spin compensation and a decrease of the spin-to-charge conversion efficiency [8]. Differently, in the surface states of a TI there is only one spin channel at negative (positive) wave vectors, hence providing a better spin-charge conversion efficiency. A similar scenario, where the Fermi contour consists of only one parallel line of opposite spin direction with respect to $\bar{\Gamma}$, has been experimentally reported for Bi high indexed surfaces [27–29], originating from the topological properties of Bi surface states.

Here, by spin-resolved photoemission experiments and first-principles calculations we show that, due to the RB effect, the Bi/Ag(110) $p(4 \times 1)$ superstructure hosts a similar, unconventional, spin texture. The present system exhibits a structural anisotropy and, at the Fermi level (E_F), a pair of states with nearly 1D contours, with only up (down) spin channel for positive (negative) wave vectors. The present superstructure provides a model system demonstrating theoretical and experimental realization of a spin texture similar to that of 1D topological materials within a RB model, offering new perspectives for 1D spin-polarized electron transport.

*daniela.pacile@fis.unical.it
†Present address: Elettra - Sincrotrone Trieste, S. S. 14 km 163.5 34149 Trieste, Italy.

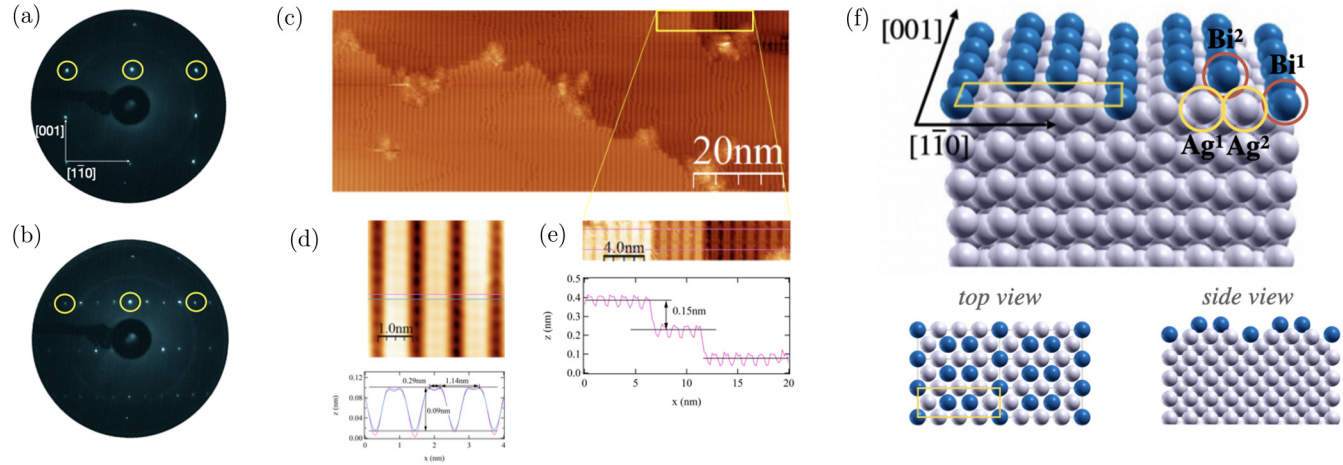

FIG. 1. LEED images taken with electron energy of 72 eV of (a) clean Ag(110); (b) Bi/Ag(110) $p(4\times1)$. (c)–(e) STM images on different length scales of the sample in (b) acquired with constant-current mode (bias voltage was −380 mV and tunneling current 1 nA). Line profiles extracted from (d) and (e) images along the pink and light blue lines, marking the apparent width and vertical displacement of the chains, as well as the step edge between adjacent Ag(110) terraces, are shown. (f) Schematics of the surface structure. The yellow rectangle is the surface unit cell. Bi^1 are Bi atoms in substitutional sites and Bi^2 in the topmost layer. Ag^1 and Ag^2 are Ag atoms of the topmost substrate layer, slightly rumpled due to the Bi atomic chains.

II. METHODS

The Ag(110) crystal was prepared by sputtering and annealing cycles. Bi was evaporated from a BN basket at a rate of 0.25 ML/min. Bi on Ag(110) forms, similarly to Bi on Cu(110), different reconstructions. Slightly below 0.5 ML the surface shows a $c(2\times2)$ reconstruction, which becomes $p(4\times1)$ at about 0.75 ML. Annealing at about 400 K for 30 min results in sharper spots and a lower background in LEED. Figure 1(b) shows the LEED pattern, where yellow circles mark the 1×1 spots of Ag(110) separated by three spots due to the $\times4$ reconstruction along the [1$\bar{1}$0] direction.

Angle-resolved photoemission spectroscopy (ARPES) measurements were performed at the VUV photoemission and at the NanoESCA [30] beamlines of the Elettra synchrotron, at $T = 90$ K, using a hemispherical analyzer and a momentum microscope, respectively. The microscope at the NanoESCA beamline is equipped with a W(001)-based spin detector [31], which enables collecting constant energy spin-resolved maps in a $[k_x, k_y]$ range of ±2 Å^{-1}. The analysis of the spin-resolved data was performed following the procedure described in [32]. The spin quantization axis (SQA) was in the surface plane, along the [001] or the [1$\bar{1}$0] direction, depending on the measurement geometry as shown in Fig. S1(a) of the Supplemental Material [33]. Additional spin-polarized ARPES spectra were acquired at the U5UA beamline at the National Synchrotron Light Source (NSLS) [34]. Scanning tunneling microscopy (STM) was conducted at the Elettra APE beamline. The topographic images were acquired in a constant current mode at RT. The calculations have been performed within density functional theory (DFT) in the generalized gradient approximation [35], employing the full potential linearized augmented planewave method as implemented in the FLEUR code [36]. For the band structure calculations we use a 20 layer Ag(110) film with the upper half relaxed and terminated with Bi rows, as shown in Fig. 1(f). The product of plane-wave cutoff and muffin-tin radius is 9.0 and 24 k-points have been used for the self-consistent calculations.

III. RESULTS AND DISCUSSION

The structural properties of the Bi/Ag(110) $p(4\times1)$ superstructure have been investigated by low energy electron diffraction (LEED) and scanning tunneling microscopy (STM). Figures 1(a) and 1(b) show the LEED patterns of clean Ag(110) and Bi/Ag(110) surfaces. The STM images, Fig. 1(c), corresponding to the LEED pattern in Fig. 1(b), shows highly oriented *single atom* chains running along the [001] direction of the substrate, regularly separated by upper *double atoms* chains, of approximately 2.9 Å lateral length [see line profile of Fig. 1(d)]. From the line profiles reported in Figs. 1(d)–1(e), the apparent vertical displacement within upper and lower Bi chains is estimated to be of about 0.9 Å and the step edge between adjacent Ag(110) terraces of about 1.5 Å, consistently with 1.45 Å expected from the bulk Ag lattice constant (or 1.46 Å calculated here from the generalized gradient approximation).

DFT, based on the STM topographic images, derives the relaxed geometry depicted in Fig. 1(f), which agrees with the experimental data. The surface unit cell (yellow rectangle) contains two types of inequivalent Bi atoms. At the corner sites of the cell, Bi atoms occupy a substitutional site in the topmost Ag layer. These alloyed atoms form parallel rows along the [001] direction, as also deduced from STM data. Between two adjacent alloyed Bi rows (Bi^1 atoms), a pair of Bi overlayer rows (Bi^2 dimers) are identified, with relative distance from Bi^1 of $\Delta z = 1.41$ Å, consistently with the atomic structure of Bi/Cu(110)[21].

In Fig. 2(a) we report ARPES data measured along $\bar{\Gamma}$-$\bar{Y}$ of the surface Brillouin zone (SBZ) of the $p(4\times1)$ superstructure, i. e., along the chain direction [001] [Fig. 2(f)] aligned with the light polarization vector (see Fig. S1a of the Supplemental Material [33]). We identify two states marked with R_1 and

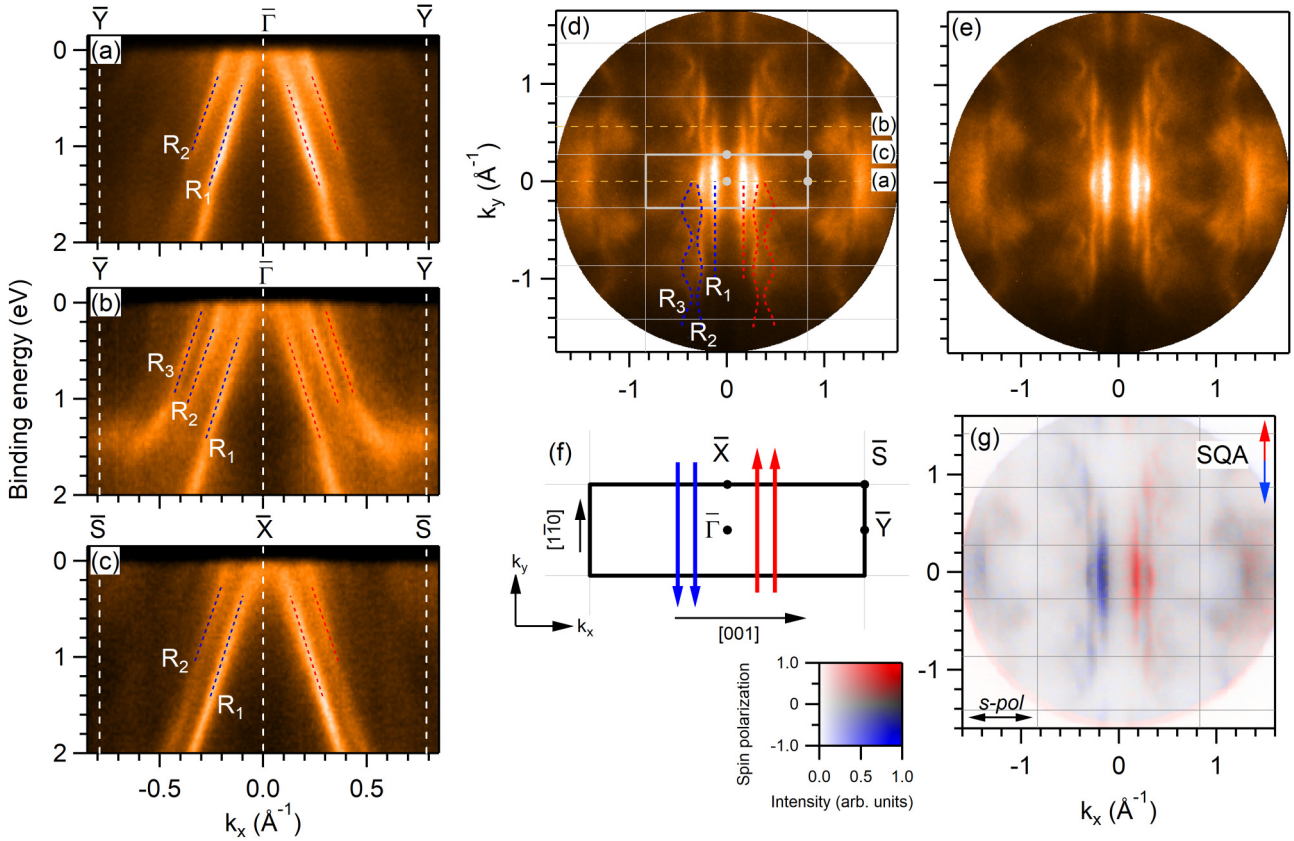

FIG. 2. Energy-momentum dispersion of Bi/Ag(110) $p(4\times1)$ along: (a) $\bar{\Gamma}$-$\bar{Y}$ of the first SBZ; (b) $\bar{\Gamma}$-$\bar{Y}$ of the second SBZ; (c) along $\bar{X}$-$\bar{S}$; the corresponding k_y positions of the cuts are indicated in (d). (d)–(e) 2D momentum maps taken at 0.55 eV binding energy with and without SBZ on top. Blue and red dashed lines indicate R_1–R_3 pair of RB states. Solid grey lines indicate the SBZ. (f) SBZ of Bi/Ag(110) $p(4\times1)$. The sketch of blue and red arrows show the spin texture at the Fermi surface from this work. (g) Spin-resolved photoemission intensities for the data shown in panel (e). Red and blue intensities correspond to spin-up and spin-down electronic states as shown in the legend. All measurements were taken at 120 eV of photon energy with *s*-polarized light. The directions of the light polarization and of the SQA are shown in panel (g).

R_2 and a third state, R_3, which is better visible in the second SBZ [Fig. 2(b)]. We mark them by blue contours on the left side of $\bar{\Gamma}$, and by red color their counterpart on the right side. Figures 2(d)–2(e) show 2D momentum maps taken at 0.55 eV binding energy. In this experimental conditions the Ag bands have a dog-bone-like shape (Fig. S1(b) of the Supplemental Material [33]), where only the part of the arclike shapes remains weakly visible. The main features arising from the Bi superstructure [Fig. 2(e)] are three states running along k_y near the center of the SBZ, corresponding to R_1, R_2, and R_3. While R_1 is nearly straight, R_2 and R_3 display a k modulation, very weak for R_2 and stronger for R_3, with a period corresponding to the SBZ periodicity. We focus on the contours of R_1 and R_2 that closely approach an ideal 1D character.

Figure 2(g) shows the spin character of the Bi-related states, measured with the SQA aligned along the $\bar{\Gamma}$-$\bar{X}$ direction (see Methods section for more details). The spin-resolved data show that the R_1 and R_2 states have an unconventional spin texture, i.e., the same spin at negative k_x, and opposite for positive k_x values. Specifically, for the R_1 state the in-plane polarization is fully along k_y, that is parallel to the Fermi contour, as confirmed by spin measurements taken with the SQA along the $\bar{\Gamma}$-$\bar{Y}$ direction (Fig. S2 of the Supplemental Material [33]). The profiles and spin polarization of the R_1 and R_2 states are similar to the ones expected for the 1D edge states of a 2D topological material. Spin-resolved ARPES on the topological metallic states of Bi(114) [27,28], display a very linear spin texture, with a single band instead of the pair in the present system. In the following, we show that although the states here observed appear very similar to the one in Refs. [27,28] their origin is different.

By changing the sample's orientation with respect to the light polarization direction (see Methods section and Fig. S1(a) of the Supplemental Material [33]) other Bi-induced states are observed, as shown in Fig. 3(a). Prominent states, R_4 and R_5 pairs, appear at higher binding energies. We notice that these states have little dispersion along $\bar{\Gamma}$-$\bar{Y}$ [Fig. 3(b)], i.e., along the chain direction. Figures 3(c)–3(d) display the spin-integrated and spin-resolved 2D momentum maps acquired at 3.0 eV binding energy [note that the SQA is now aligned along $\bar{\Gamma}$-$\bar{Y}$, as shown in Fig. 3(e)], showing the contours of R_5 state repeated according to $\times4$ periodicity. We notice an unconventional spin pattern with one spin channel above $\bar{\Gamma}$ and opposite below, as sketched in Fig. 3(e). A similar texture is observed also for the R_4 state (Fig. S3 in the Supplemental Material [33]).

In order to discuss these findings, we present DFT calculations for the electronic states of the Bi/Ag(110) $p(4\times1)$ system along the chain direction $\bar{\Gamma}$-$\bar{Y}$ [Fig. 4(a)]. We observe four pairs of nearly parabolic spin-orbit split bands crossing

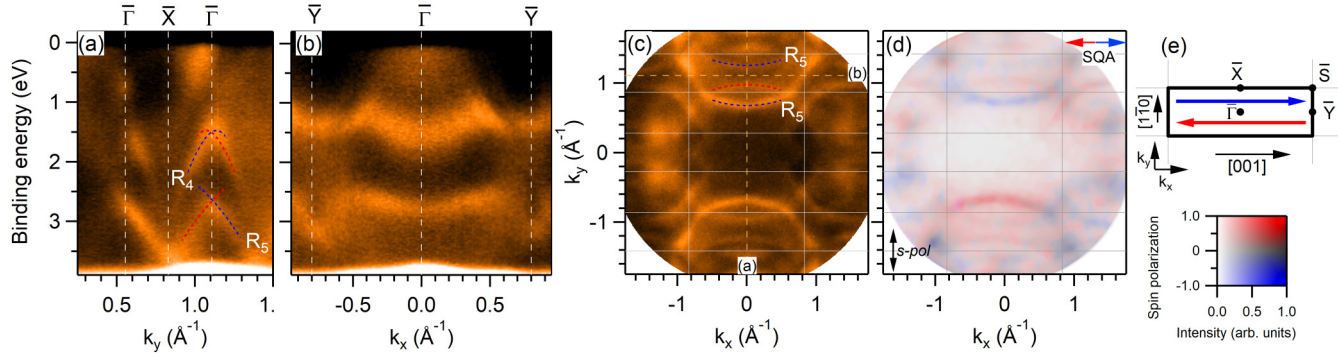

FIG. 3. (a), (b) Energy-momentum dispersion of Bi/Ag(110) $p(4\times1)$: (a) along $\bar{\Gamma}$-$\bar{X}$ direction; (b) along $\bar{\Gamma}$-$\bar{Y}$ direction. The corresponding k_y and k_x positions of the cuts are indicated in the panel (c). (c) 2D momentum map, taken at 3.0 eV binding energy. (d) Spin-resolved photoemission intensities of the data shown in panel (c). Blue and red dashed lines indicate R_4–R_5 pair of RB states. Solid grey lines indicate the SBZ. All measurements were taken at 120 eV of photon energy with *s*-polarized light. (e) SBZ of Bi/Ag(110) $p(4\times1)$. The sketch of blue and red arrows show the spin texture at about 3.0 eV binding energy from this work.

at $\bar{\Gamma}$ at 0.1, −0.2, −1.0 and −1.7 eV. We identify with R_1, R_2, R_3 the lowest three pairs of bands. These bands correspond to the experimentally observed R_1, R_2, and R_3 states beside a discrepancy in the energy position, both along $\bar{\Gamma}$-$\bar{Y}$ and $\bar{X}$-$\bar{S}$ directions [Fig. S4(a) in the Supplemental Material [33] shows theoretical results along $\bar{X}$-$\bar{S}$ direction]. In agreement with the experiment, R_1 and R_2 states are the most intense features with same position in k_x between $\bar{\Gamma}$-$\bar{Y}$ and $\bar{X}$-$\bar{S}$ direction, leading to nearly linear contours in the constant energy cuts. On the other hand, the binding energy position of R_3 varies, leading to the observed undulations. Focusing on the second pair, R_2, from a parabolic fit around the vertex, we extract a shift of the band maximum away from Γ point of about $k_0 = 0.035$ Å^{-1}, corresponding to a Rashba parameter of $\alpha = 1.65$ eVÅ and comparable to the giant spin splitting of the $Bi_xPb_{1-x}Ag_2$ surface alloy [37]. Moreover, the k_0 value here extracted is close to the maximum momentum splitting measured at the border of the BZ in the Bi/Cu(110) $p(4\times1)$

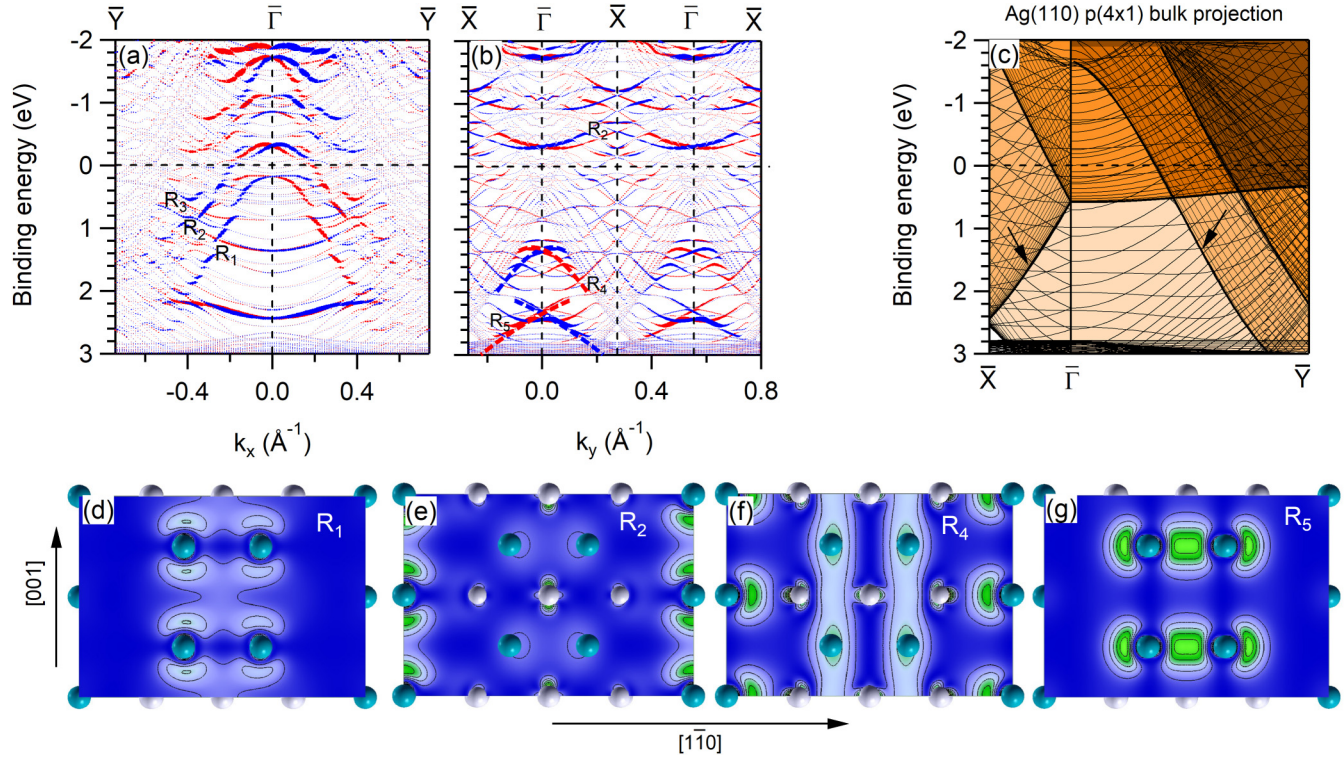

FIG. 4. (a) Theoretical band structure of Bi/Ag(110) $p(4\times1)$ parallel to the Bi chains, that is along $\bar{\Gamma}$-$\bar{Y}$. The color and size of the symbols indicate the orientation and size of the spin-polarization at the Bi atoms in the k_y direction. (b) The same representation perpendicular to the Bi chains, i. e., along $\bar{\Gamma}$-$\bar{X}$, with SQA referred to k_x direction. (c) Ag(110) bands along $\bar{\Gamma}$-$\bar{X}$ and $\bar{\Gamma}$-$\bar{Y}$ folded according to the 4 × 1 periodicity. Different colors indicate a different density of states. (d)–(g) Charge density plots of states R_1 (d), R_2 (e), R_4 (f), and R_5 (g) pairs in the plane of the Bi^2 dimers (d), (g) or the Bi^1 alloyed atoms (e), (f). (d), (e) are extracted at 0.6 eV; (f) at 1.4 eV; (g) at 2.3 eV binding energy. Bi atoms are shown in blue, Ag atoms in grey.

system, $2k_0 = (0.075 \pm 0.05)$ Å^{-1}[21]. In Fig. 4(a) we also notice two weakly dispersive states with positive effective mass, located at $\bar{\Gamma}$ point at about 1.4 and 2.4 eV, respectively. They are clearly visible in the experimental results of Fig. 3(b) and correspond to R_4 and R_5 states, beside a discrepancy in the energy position.

In Fig. 4(b) we show the theoretical band structure in the perpendicular direction [1$\bar{1}$0], i.e., along $\bar{\Gamma}$-$\bar{X}$. The R_2 pair crosses above E_F and form two parabola with positive effective mass. We can estimate a Rashba parameter of about $\alpha = 0.55$ eVÅ, much smaller than the one extracted along the $\bar{\Gamma}$-$\bar{Y}$ direction, where there is higher group velocity. We furthermore notice that the R_2 pair shows a saddlelike shape in k space, similar to what has been observed in deeply lying RB split Ag(111) and Au(111) surface states located at $\bar{M}$ [38]. In the binding energy range between 0 and 1 eV below E_F, the R_1-R_3 states form open contours, thus we only observe Ag states arising from the $\times 4$ folding. Above 1.0 eV binding energy, in line with the experimental results of Fig. 3, we find several spin-split bands belonging to Bi, among which we select the R_4 and R_5 pairs with crossing point at about 1.4 and 2.3 eV, respectively. As a result of the comparison with Fig. 4(a), we point out that these deeper lying states are mainly dispersive along the perpendicular direction, where, indeed, they exhibit sizable RB splitting and higher group velocity. Instead, in agreement with the experiment, these states are nearly nondispersive along $\bar{\Gamma}$-$\bar{Y}$ [Fig. 4(a)], and cause the observed kinks when intersecting the higher Bi states, as seen in Figs. 2(a) and 3(b).

DFT calculations explain the origin of the particular spin texture for R_1 and R_2, as well as for R_4 and R_5 states. In Fig. 4(c) we show surface projected Ag(110) bands folded according to the 4×1 periodicity. Here, a steplike increase in the density of Ag states is expected going farther from the $\bar{\Gamma}$ point, both along the $\bar{\Gamma}$-$\bar{X}$ and $\bar{\Gamma}$-$\bar{Y}$ directions. Several zones with different density of states can be identified, as highlighted by different color. A bright zone close to $\bar{\Gamma}$, delimited by two lines marked by black arrows, has relatively low density of Ag states. When Bi atoms are accounted for, the inner branch of a RB pair (e.g., R_1 at negative wave vectors) remains within this zone and has little hybridization with Ag states. The outer branch (such as R_1 at positive wave vectors) due to its lower group velocity enters the zone with dense Ag states, just below E_F, thus hybridizing with the Ag states. For this reason, both along $\bar{\Gamma}$-$\bar{X}$ and $\bar{\Gamma}$-$\bar{Y}$, for each pair of Bi states the inner spin-split band is visible in the simulations as well as in the experiments, while the outer one strongly hybridizes with the Ag bulk states, leading to one single band for positive (negative) k values.

Figures 4(d)–4(g) show charge density plots of the Bi-derived states, all having p character. The R_1 and R_2 states are oriented along the chain direction [001] [Figs. 4(d) and 4(e)], and exhibit 1D dispersion character. We point out that the R_1 state is localized on Bi dimer rows, while the R_2 state is centered on the alloyed Bi rows. We notice that R_1 state, at variance with R_2, shows a significant hybridization with the Ag states (see Fig. S4(b) and S4(c) of the Supplemental Material [33]). The R_4 and R_5 are mainly oriented along the [1$\bar{1}$0] direction [Figs. 4(f) and 4(g)]. The R_5 is fully localized at Bi^2 dimers along [1$\bar{1}$0] direction and with small overlap along the chains direction. The R_4 shows a more complex behavior, mostly located at Bi^1 alloyed atoms but with non-negligible extension along both directions. The strong anisotropy of Bi states shown here explains why by changing the light polarization one can selectively excite one pair (R_1 and R_2 in Fig. 2) or the other (R_4 and R_5 in Fig. 3).

Finally, we comment on the perspectives of the present results for spintronics applications. The present superstructure provides a model system demonstrating theoretical and experimental realization of unconventional spin texture, similar to that of 1D topological materials, within a RB model. Our study may stimulate further exploration of similar systems being useful for energy-efficient spintronic applications.

IV. CONCLUSIONS

We report on quasi-1D atomic and electronic structure with unconventional RB spin texture observed in Bi/Ag(110) $p(4\times1)$ superstructure. Using ARPES we show that the Fermi surface displays a pair of linear states strongly localized on the chains and dispersing along the chain direction. Spin-resolved photoemission spectroscopy on these states shows that only up (down) spin channel is present at positive (negative) wave vectors. We support our findings by DFT calculations, which explain the current spin texture as originating from the k-dependent hybridization of the Bi-derived RB bands with the Ag bulk states. The present nonconventional spin texture, together with quasi-1D shape, may support the realization of spintronic devices based on spin-charge interconversion.

ACKNOWLEDGMENTS

We acknowledge EUROFEL-ROADMAP ESFRI of the Italian Ministry of Education, University, and Research. G.B. gratefully acknowledges the computing time granted through JARA-HPC on the supercomputer JURECA at Forschungszentrum Jülich. This work is supported by the German Federal Ministry of Education and Research (BMBF) under Grant No. 05K19PGA. Part of this work has been performed in the framework of the nanoscience foundry and fine analysis (NFFA-MIUR Italy, Progetti Internazionali) facility.

[1] S. Datta and B. Das, Appl. Phys. Lett. **56**, 665 (1990).

[2] D. D. Awschalom and M. E. Flatté, Nat. Phys. **3**, 153 (2007).

[3] P. Chuang, S.-C. Ho, L. W. Smith, F. Sfigakis, M. Pepper, C.-H. Chen, J.-C. Fan, J. P. Griffiths, I. Farrer, H. E. Beere, G. A. C. Jones, D. A. Ritchie, and T.-M. Chen, Nat. Nanotechnol. **10**, 35 (2015).

[4] H. C. Koo, J. H. Kwon, J. Eom, J. Chang, S. H. Han, and M. Johnson, Science **325**, 1515 (2009).

[5] I. Appelbaum, B. Huang, and D. J. Monsma, Nature (London) **447**, 295 (2007).

[6] J. C. R. Sánchez, L. Vila, G. Desfonds, S. Gambarelli, J. P. Attané, J. M. De Teresa, C. Magén, and A. Fert, Nat. Commun. **4**, 2944 (2013).
[7] E. Lesne, Y. Fu, S. Oyarzun, J. C. Rojas-Sánchez, D. C. Vaz, H. Naganuma, G. Sicoli, J. P. Attané, M. Jamet, E. Jacquet, J. M. George, A. Barthélémy, H. Jaffrès, A. Fert, M. Bibes, and L. Vila, Nat. Mater. **15**, 1261 (2016).
[8] R. Sun, S. Yang, X. Yang, E. Vetter, D. Sun, N. Li, L. Su, Y. Li, Y. Li, Z.-z. Gong, Z.-k. Xie, K.-y. Hou, Q. Gul, W. He, X.-q. Zhang, and Z.-h. Cheng, Nano Lett. **19**, 4420 (2019).
[9] Y. Shiomi, K. Nomura, Y. Kajiwara, K. Eto, M. Novak, K. Segawa, Y. Ando, and E. Saitoh, Phys. Rev. Lett. **113**, 196601 (2014).
[10] J.-C. Rojas-Sánchez, S. Oyarzún, Y. Fu, A. Marty, C. Vergnaud, S. Gambarelli, L. Vila, M. Jamet, Y. Ohtsubo, A. Taleb-Ibrahimi, P. Le Fèvre, F. Bertran, N. Reyren, J.-M. George, and A. Fert, Phys. Rev. Lett. **116**, 096602 (2016).
[11] J. Han, A. Richardella, S. A. Siddiqui, J. Finley, N. Samarth, and L. Liu, Phys. Rev. Lett. **119**, 077702 (2017).
[12] K. Kondou, R. Yoshimi, A. Tsukazaki, Y. Fukuma, J. Matsuno, K. S. Takahashi, M. Kawasaki, Y. Tokura, and Y. Otani, Nat. Phys. **12**, 1027 (2016).
[13] R. Noguchi, T. Takahashi, K. Kuroda, M. Ochi, T. Shirasawa, M. Sakano, C. Bareille, M. Nakayama, M. D. Watson, K. Yaji, A. Harasawa, H. Iwasawa, P. Dudin, T. K. Kim, M. Hoesch, V. Kandyba, A. Giampietri, A. Barinov, S. Shin, R. Arita *et al.*, Nature (London) **566**, 518 (2019).
[14] R. Noguchi, M. Kobayashi, Z. Jiang, K. Kuroda, T. Takahashi, Z. Xu, D. Lee, M. Hirayama, M. Ochi, T. Shirasawa, P. Zhang, C. Lin, C. Bareille, S. Sakuragi, H. Tanaka, S. Kunisada, K. Kurokawa, K. Yaji, A. Harasawa, V. Kandyba *et al.*, Nat. Mater. **20**, 473 (2021).
[15] L. Qiao, X. Xiong, H. Yang, D. Chen, Y. Li, J. Li, X. Peng, Z. Xu, J. Han, W. Xiao, and Y. Yao, J. Phys. Chem. C **125**, 22312 (2021).
[16] J. I. Pascual, G. Bihlmayer, Y. M. Koroteev, H.-P. Rust, G. Ceballos, M. Hansmann, K. Horn, E. V. Chulkov, S. Blügel, P. M. Echenique, and P. Hofmann, Phys. Rev. Lett. **93**, 196802 (2004).
[17] P. Segovia, D. Purdie, M. Hengsberger, and Y. Baer, Nature (London) **402**, 504 (1999).
[18] D. Sánchez-Portal, S. Riikonen, and R. M. Martin, Phys. Rev. Lett. **93**, 146803 (2004).
[19] I. Barke, F. Zheng, T. K. Rügheimer, and F. J. Himpsel, Phys. Rev. Lett. **97**, 226405 (2006).
[20] T. Nakamura, Y. Ohtsubo, Y. Yamashita, S.-i. Ideta, K. Tanaka, K. Yaji, A. Harasawa, S. Shin, F. Komori, R. Yukawa, K. Horiba, H. Kumigashira, and S.-i. Kimura, Phys. Rev. B **98**, 075431 (2018).
[21] A. Crepaldi, G. Bihlmayer, K. Kern, and M. Grioni, New J. Phys. **15**, 105013 (2013).
[22] A. Crepaldi, C. Tournier-Colletta, M. Pivetta, G. Autès, F. Patthey, H. Brune, O. V. Yazyev, and M. Grioni, Phys. Rev. B **88**, 195433 (2013).
[23] Y. Ohtsubo, N. Tokumasu, H. Watanabe, T. Nakamura, P. Le Fèvre, F. Bertran, M. Imamura, I. Yamamoto, J. Azuma, K. Takahashi, and S.-I. Kimura, Phys. Rev. B **101**, 235306 (2020).
[24] J. Park, S. W. Jung, M.-C. Jung, H. Yamane, N. Kosugi, and H. W. Yeom, Phys. Rev. Lett. **110**, 036801 (2013).
[25] M. Kopciuszyński, M. Krawiec, R. Zdyb, and M. Jaochowski, Sci. Rep. **7**, 46215 (2017).
[26] A. N. Mihalyuk, L. V. Bondarenko, A. Y. Tupchaya, T. V. Utas, Y. E. Vekovshinin, D. V. Gruznev, S. V. Eremeev, A. V. Zotov, and A. A. Saranin, Phys. Rev. B **104**, 125413 (2021).
[27] P. Hofmann, M. M. Ugeda, A. Tamtögl, A. Ruckhofer, W. E. Ernst, G. Benedek, A. J. Martínez-Galera, A. Stróżecka, J. M. Gómez-Rodríguez, E. Rienks, M. F. Jensen, J. I. Pascual, and J. W. Wells, Phys. Rev. B **99**, 035438 (2019).
[28] J. W. Wells, J. H. Dil, F. Meier, J. Lobo-Checa, V. N. Petrov, J. Osterwalder, M. M. Ugeda, I. Fernandez-Torrente, J. I. Pascual, E. D. L. Rienks, M. F. Jensen, and P. Hofmann, Phys. Rev. Lett. **102**, 096802 (2009).
[29] M. Bianchi, F. Song, S. Cooil, A. F. Monsen, E. Wahlström, J. A. Miwa, E. D. L. Rienks, D. A. Evans, A. Strozecka, J. I. Pascual, M. Leandersson, T. Balasubramanian, P. Hofmann, and J. W. Wells, Phys. Rev. B **91**, 165307 (2015).
[30] C. Schneider, C. Wiemann, M. Patt, V. Feyer, L. Plucinski, I. Krug, M. Escher, N. Weber, M. Merkel, O. Renault, and N. Barrett, J. Electron Spectrosc. Relat. Phenom. **185**, 330 (2012).
[31] C. Tusche, M. Ellguth, A. A. Ünal, C.-T. Chiang, A. Winkelmann, A. Krasyuk, M. Hahn, G. Schönhense, and J. Kirschner, Appl. Phys. Lett. **99**, 032505 (2011).
[32] C. Tusche, M. Ellguth, A. Krasyuk, A. Winkelmann, D. Kutnyakhov, P. Lushchyk, K. Medjanik, G. Schönhense, and J. Kirschner, Ultramicroscopy **130**, 70 (2013), Eighth International Workshop on LEEM/PEEM.
[33] See Supplemental Material at http://link.aps.org/supplemental/10.1103/PhysRevB.106.045108 for the description of the experimental geometry, as well as additional DFT calculations and ARPES data.
[34] E. Vescovo, H.-J. Kim, Q.-Y. Dong, G. Nintzel, D. Carlson, S. Hulbert, and N. V. Smith, Synchrotron Radiation News **12**, 10 (1999).
[35] J. P. Perdew, K. Burke, and M. Ernzerhof, Phys. Rev. Lett. **77**, 3865 (1996).
[36] For a program description see https://www.flapw.de.
[37] C. R. Ast, D. Pacilé, L. Moreschini, M. C. Falub, M. Papagno, K. Kern, M. Grioni, J. Henk, A. Ernst, S. Ostanin, and P. Bruno, Phys. Rev. B **77**, 081407(R) (2008).
[38] R. Requist, P. M. Sheverdyaeva, P. Moras, S. K. Mahatha, C. Carbone, and E. Tosatti, Phys. Rev. B **91**, 045432 (2015).